

FATIGUE DAMAGE OF 2024-T351 ALUMINIUM ALLOY FRICTION STIR WELDING JOINTS. PART 1: CHARACTERISATION

Aidy Ali^{1*}, Mike W. Brown², and Omar Suliman Zaroog¹

Received: Jan 22, 2008; Revised: May 21, 2008; Accepted: May 21, 2008

Abstract

Characterisation of macrostructure, microstructure, hardness, residual stress and cyclic deformation behaviour of 2024-T351 Aluminium Alloy FSW joints has been conducted in order to characterise the critical areas for fatigue crack initiation. Inhomogeneous micro-parameters that govern the non-uniform residual stresses and cyclic strength are then discussed. The cyclic strength of the weld micro-regimes are controlled by grain size and distribution of precipitates achieved during the weld process. The comprehensive information of micro and macro mechanics gathered is used to assist in understanding the mechanism that governed the fatigue crack initiation, propagation, and life of this weld.

Keywords: 2024-T351 Aluminium alloy, fatigue, friction stir welding (FSW)

Introduction

Friction stir welding is a solid state welding process that has received worldwide attention, particularly for joining aluminium alloys (Dawes, 1995; Williams, 2001). There have been numerous attempts on characterisation in terms of macrostructure, microstructure, hardness and residual stress distribution in connection with the FSW of aluminium alloys such as 2024 (Dalle Donne and Biallas, 1999; Booth and Sinclair, 2002; Sutton *et al.*, 2002; Bussu and Irving, 2003), 7075 (Mahoney *et al.*, 1998), 7050 (Jata *et al.*, 2000),

6061 (Murr *et al.*, 1998), 6013 (Heinz *et al.*, 2000), 6063 (Sato and Kokawa, 2001), 1050 (Kwon *et al.*, 2002), 1100 (Murr *et al.*, 1998; Flores *et al.*, 1998), and 1080 and 5083 (Sato *et al.*, 2001). Nevertheless there has been no systematic attempt to investigate the natural crack initiation site in FSW.

In this paper, the comprehensive characterisations of micro and macro mechanics of FSW 2024-T351 were performed based on the macrostructure, microstructure, hardness,

¹ Fatigue and Fracture Research Group, Department of Mechanical and Manufacturing Engineering, University of Putra Malaysia, 43400 Serdang, Selangor, Malaysia. E-mail: aidy@eng.upm.edu.my

² Department of Mechanical Engineering, The University of Sheffield, Mappin Street, Sheffield, S1 1JD, United Kingdom.

* Corresponding author

residual stress, and cyclic deformation behaviour. The experimental procedure that is used to extract the information of the characterisation work is detailed. With systematic characterisation, the information gathered will be used to assist in modelling the effect of the macrostructure, microstructure, hardness, residual stress, and cyclic strength on the fatigue behaviour of FSW in connection with the natural crack initiation site, propagation, and life.

Experimental Procedure

The investigation was performed on a 13 mm thick plate of 2024-T351 Al Alloy. The FSW was provided by Airbus UK Ltd. Chester Manchester. Plates $75 \times 60 \times 13$ mm were welded along their long edge with the weld direction parallel to the longitudinal (rolling) orientation.

Welds was characterised in terms of their macrostructure, microstructure, hardness, residual stress, and cyclic deformation behaviour. For optical observation purposes, cross sections of the welds were mechanically polished to a $\frac{1}{4}$ micron finish and lightly etched in Keller's reagent in accordance with ASTM E340-00 (1999). Hardness measurements were in accordance with ASTM E92-82(1989). Residual stresses were measured in a longitudinal welded specimen after surface skimming about 0.5 mm thick. The measurements used the hole-drilling strain gauge techniques in accordance with ASTM E837-99(2000). In order to determine the longitudinal residual stresses through the thickness of the weld, the slicing and layer removal techniques with a compliment of deformation strain gauges were applied to the back of the test specimen to measure the deformation along the longitudinal and transverse directions. The longitudinal and transverse residual stresses were calculated by using the following equations (Lu, 1996):

$$\sigma_1(e) = \frac{E}{1-\nu} \left(-\frac{1}{2} e \frac{d_{i_1}}{d_e} + i_1 - 3e \int \frac{d_{i_1}}{e} \right) \quad (1)$$

$$\sigma_2(e) = \frac{E}{1-\nu} \left(-\frac{1}{2} e \frac{d_{i_2}}{d_e} + i_2 - 3e \int \frac{d_{i_2}}{e} \right) \quad (2)$$

$$\begin{aligned} \text{where } i_1 &= \varepsilon_x + \nu \varepsilon_y \\ i_2 &= \varepsilon_y + \nu \varepsilon_x \end{aligned}$$

$\sigma_1(e)$ = longitudinal residual stresses, $\sigma_2(e)$ = transverse residual stresses, h = initial thickness, e = remaining thickness after removal, de = removed layer thickness, e' = thickness of removed layer + de , ν = Poison's ratio, E = modulus of elasticity, $d_{i_1} = i_{1_{after}} - i_{1_{before}}$, $d_{i_2} = i_{2_{after}} - i_{2_{before}}$, ε_x = deformation along the transverse axis after removal, and ε_y = deformation along the longitudinal axis after removal.

In order to investigate the cyclic deformation behaviour for each microstructural regime in FSW, fully reversed pure cyclic bending tests were performed under displacement control for strain ranges 0.1% and 2.5%. The value for the total cyclic strain, ε , and surface cyclic stress, σ , were calculated by the following equation (Nadai, 1950):

$$\varepsilon = \frac{2\Phi y}{L} \quad (3)$$

$$\sigma = \frac{M}{\frac{2b}{n+2}(y^2)} \quad (4)$$

where y = the vertical distance from the centroid of the specimen, Φ = the half-angle of the bend, L = the specimen gauge length, M = the bending moment, n = the strain hardening exponent, and b = the specimen thickness.

Experimental Result

Macrostructure

Figure 1(a) shows a transverse macro-section of a FSW joint. The most obvious feature is the weld-defined nugget (N) in the centre of the weld. On top of the N, it is possible to identify a flow arm (FA) region between the N and the top surface on which welding was carried out.

Further out, about 10 mm from the plate joint line (PJL) is the thermo-mechanically affected zone (TMAZ). The size of this region is up to 4.0 mm wide on the top welding surface and it narrows down throughout the thickness of the 10.5 mm of the plate. Next to the TMAZ region is the heat affected zone (HAZ). The size of this region is up to 4 mm narrow on the top welding surface and it widens down throughout the thickness of the plate. It is worth noting that the TMAZ region is absent on the bottom of the weld and the entire region's size is not symmetrical on both the right and left sides due to the pin rotational direction. The coordinate boundaries of each macrostructural zone were mapped by using optical PolyVarMet microscopy as shown in Figure 1(b).

Microstructure

Figure 2 represents a microstructure of a FSW joint for each region. The finest microstructure size is found in the N region with a

microstructure size of the order of 5 - 10 μm . The FA region also has a fine equiaxed grain structure up to 15 μm , close to the microstructure size as in the N region. It is worth noting that the microstructure presence in the TMAZ was an elongated grain structure which is believed to be due to severe plastic deformation which takes place during welding and the stirring action causes the flat grains of the parent metal to be drawn into the weld nugget zone. The grain size in the TMAZ is about 200 - 400 μm , slightly bigger than the parent material. The grain structure in the HAZ and parent plate appears to have a similar size in the order of 150 - 200 μm . The anomaly of the grain size in each region depends on the material and process parameters of the FSW joint itself. The non-uniform microstructure existing in the FSW joints is believed to have led to having a different fatigue strength for each zone of the weld.

Hardness

Figure 3 shows hardness profiles measured on the top and bottom surfaces across the weld. Obviously the hardness on the top and the bottom

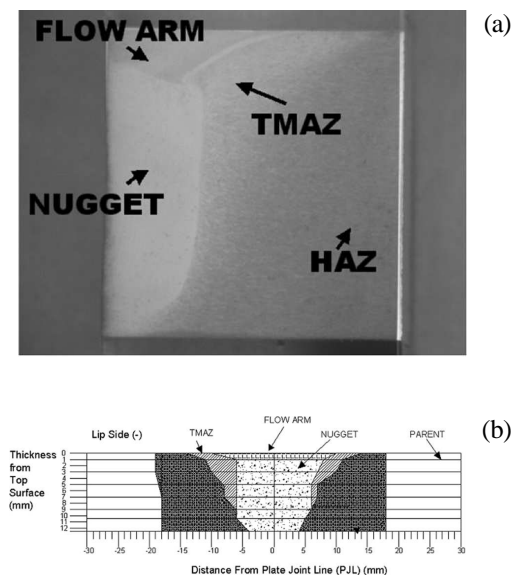


Figure 1. The transverse cross section in an as-welded FSW 2024-T351 Al Alloy joint and the mapping of boundaries between each macrostructural zone

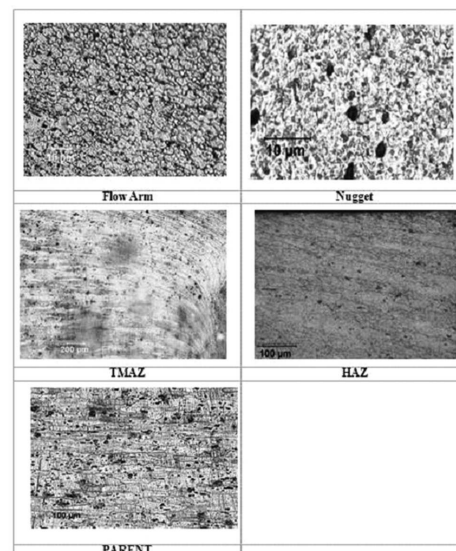


Figure 2. The microstructures of a FSW joint for each macro structural region

were not similar due to having the different macrostructure and microstructure. The hardness on the bottom weld is lower than the top, especially in the N region. The lowest hardness was found at the boundary between the TMAZ and HAZ regions which was about 118 Hv1 in the range of 11 - 14 mm from the PJJ. The hardness increases towards the N with a slight decrease for the area closest to the PJJ. The highest hardness was found in the HAZ region which was about 167 Hv1 in the range of 18 - 21 mm from the PJJ. The parent material hardness is constant; it fluctuates due to partial recrystallisation in the range of 25 - 100 mm from the PJJ.

In order to investigate a possible variation of hardness from the top surface through the depth, a microhardness test was performed on several profiles at different distances from the PJJ as shown in Figure 4(a). Six profiles numbered 1 - 6 were chosen based on different microstructural types as shown in Figure 4(a), where the profiles 1 and 2 were located in the N region, profile 3 was in the FA, TMAZ, and HAZ regions, profiles 4 and 5 were in the HAZ region and profile 6 is in the parent plate region. Figure 4(b) shows a microhardness result through the depth of the FSW for the entire six profiles. It can be seen that, the hardness in profile 1 gradually decreases towards the depth, whilst in profile 3 the hardness begins with 135 Hv_{0.1} in the FA region then decreases to 110 Hv_{0.1} when

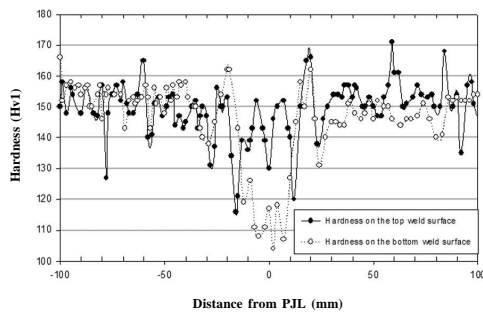


Figure 3. Vickers hardness traverse across the FSW 2024-T351 Al Alloy joint at various positions in the section

it goes to the TMAZ region; after that it gradually increases towards the depth in the HAZ region. The hardness in profiles 4, 5, and 6 were constant and there is no significant drop when it approaches towards the depth.

Residual Stress

Figure 5(a) shows the position where the hole was drilled for measuring the residual stress on the top and bottom of the weld. Figure 5(b) shows the longitudinal residual stress profile along the weld measured from the top and bottom sides of the weld. It is worth noting that the longitudinal residual stress reveals an 'M'-like shape and it agrees with many previous findings on characterising the residual stress in FSW. Residual stress found on the top and the bottom surfaces of the weld were not similar. On the top of the weld the residual stress is highly tensile at a position of -12 mm from the PJJ, which is about 95 MPa, and it was located in the TMAZ region. Tensile residual stress also found at 12 mm from the PJJ, which is about 46 MPa, and it also fall in the TMAZ region.

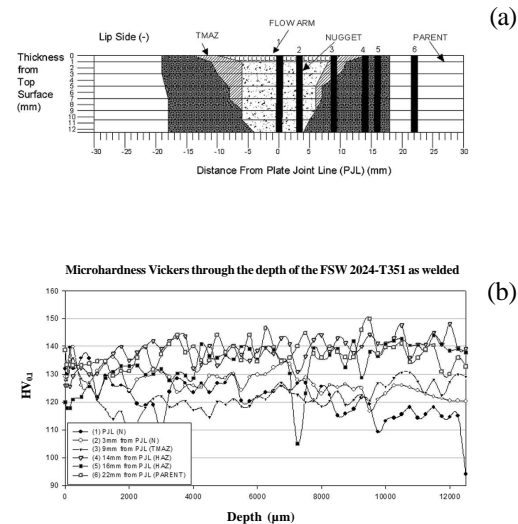


Figure 4. Microhardness Vickers through the depth of the FSW 2024-T351 Al Alloy joint at several distances from PJJ

From these two locations the tensile residual stresses decrease in the parent plate adjacent to the HAZ as well as the N, which contains compressive residual stresses at about -41 MPa. With increasing distance from the PJJ, the residual stress then gradually changes into the initial stress state of the parent material which is about zero. On the other hand, the bottom side residual stress was compressive at -17 and 17 mm from the PJJ which is about -40 MPa and -50 MPa respectively, and it was located in the HAZ region. The maximum tensile residual stress in the bottom side was found at -7 mm from PJJ about 25 MPa which is located in HAZ region. In order to investigate the residual stress further through the depth, the specimens were sliced into small strips as shown in Figure 6(a). The strain gauges were placed at the back of each strip and the layers were removed gradually with a 1 mm depth rate of removal. Figure 6(b) shows the residual stress profile throughout the depth of the weld. The surface residual stress was agreed with the hole drilling technique. The residual stress gradually decreases from high

tension to compression when it approach the mid section of the thickness.

Cyclic Deformation Behaviour

In cyclic bending tests, the specimens were cut-off from each microstructural regime with different cross section sizes as shown on Figure 7(a). The specimens were numbered according to their regime as N, Composite of TMAZ and HAZ, HAZ, and Parent plate with number 1, 2, 3, and 4. Figure 7(b) shows the photograph

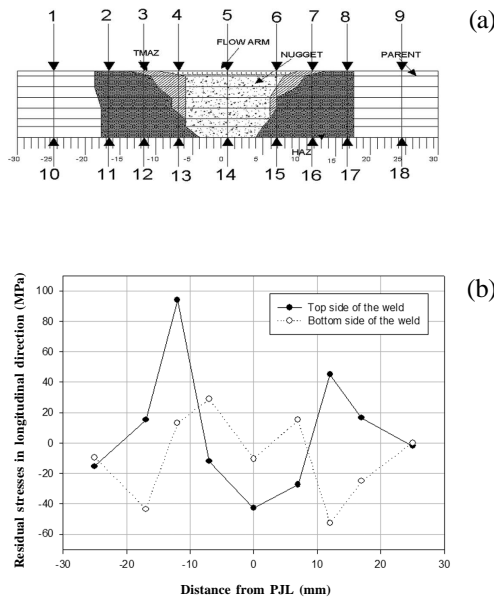


Figure 5. The residual stress profile along the FSW 2024-T351 Al Alloy weld

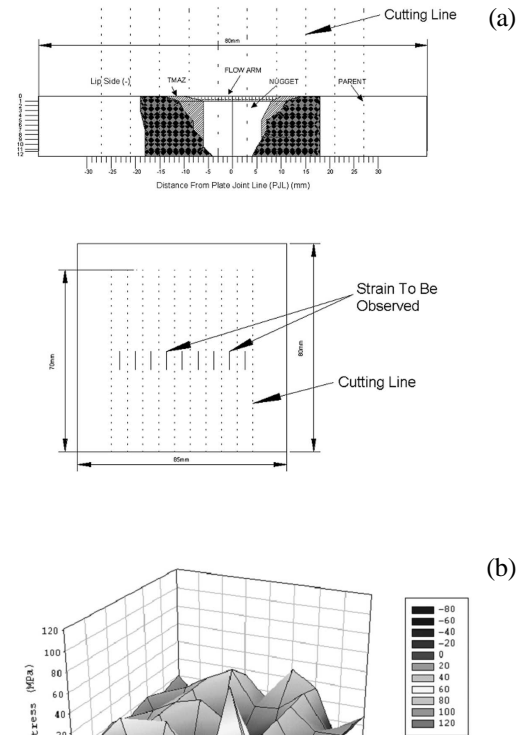


Figure 6. Slicing scheme and the residual stress profile in the FSW 2024-T351 through the depth obtained from the Layer Removal Technique

showing the specimen clamped on the bending machine. The A hysteresis loops plotted by X-Y plotter for Parent FSW plate is shown in Figure 8. A cyclic stress strain curves generated for Parent regime in FSW 2024-T351 Al Alloy is shown in Figure 9. Plain strain fracture surface was obtained as shown in Figure 10.

The work considered the rectangular cross-section specimen subjected to a reversed bending moment M and assume that original plane sections remain plane under bending. The amplitude of surface strain at a distance y from the neutral axis of the specimen is given by

$$\varepsilon = \frac{2\Phi y}{L} \tag{5}$$

where y = the vertical distance from the centroid of the specimen, Φ = the half-angle of bend and L = the specimen gauge length.

The total bending moment, taking into account the symmetrical contribution to the bending moment of the sections above and below the neutral axis is

$$M = 2 \int_0^{y_{max}} \sigma y b dy \tag{6}$$

where b = the specimen thickness. Because of the non-linear stress-strain behaviour, the material is assumed to follow a power law

$$\sigma = k(\varepsilon)^n \tag{7}$$

Expressing the stress in terms of its equivalent strain from Eqns. (5) and (7) gives

$$M = 2 \int_0^{y_{max}} k(\varepsilon)^n y b dy \tag{8}$$

$$M = 2 \int_0^{y_{max}} k \left(\frac{2\Phi y}{L} \right)^n y b dy \tag{9}$$

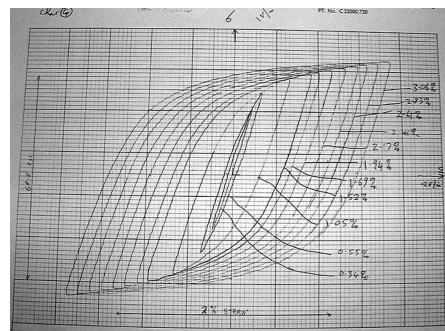
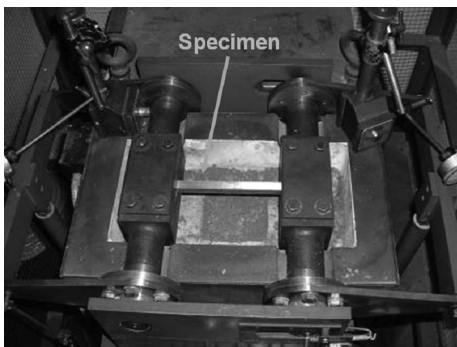
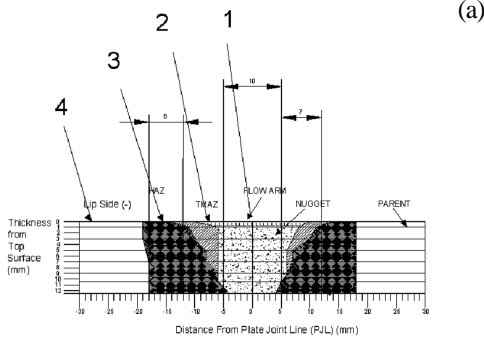


Figure 7. Cutting scheme and photograph of specimen loaded on the bending cyclic machine

Figure 8. A hysteresis loops plotted by X-Y plotter for Parent FSW plate

Integration to the limit of $y = y_{max}$ in Eqn. (9), the maximum bending moment is expressed as

$$M = \frac{2bk}{n+2} \left(\frac{2\Phi}{L} \right)^n y_{max}^{n+2} \tag{10}$$

Since

$$\sigma_{max} = k \left(\frac{2\Phi y_{max}}{L} \right)^n \tag{11}$$

where σ_{max} is the maximum surface tensile stress, knowing the hardening exponent n , it can be computed as follows

$$\sigma_{max} = \frac{M}{\frac{2b}{n+2} (y_{max}^2)} \tag{12}$$

Results from the cyclic pure bending tests are summarised in Table 1. Following a regression of all the data points, Ramberg-Osgood type equations in terms of, respectively, the elastic and inelastic strain range were produced:

Table 1. The result of cyclic tests in pure bending

Regimes	Modulus of Elasticity (E) GPa	Strain Hardening Exponent (n)	Hardening Constant (H) -----MPa-----	Cyclic Yield Strength (σ_0)
Parent Material	68	0.086	770	340
HAZ	68	0.055	719	410
TMAZ	68	0.1413	800	250
(Composite 35% TMAZ+ 65% HAZ)				
N	68	-	-	-

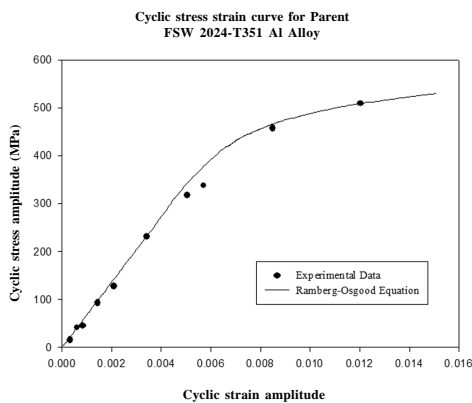


Figure 9. Cyclic stress strain curves of Parent regime in FSW 2024-T351 Al Alloy

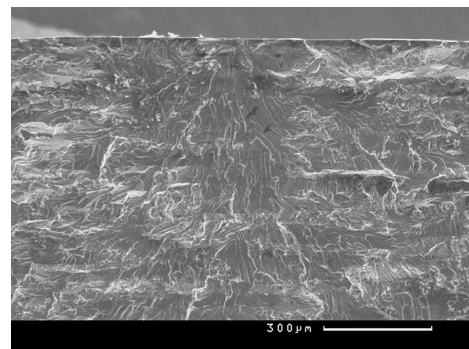


Figure 10. Smooth flat fracture surface of broken sample show a plain strain controlled

$$\varepsilon = \varepsilon_e + \varepsilon_p \quad (13)$$

$$\sigma = H\varepsilon_p^n \quad (14)$$

$$\text{give } \varepsilon = \frac{\sigma}{E} + \left(\frac{\sigma}{H}\right)^{\frac{1}{n}} \quad (15)$$

where ε = total cyclic strain, ε_e = cyclic elastic strain, ε_p = cyclic plastic strain, σ = cyclic stress, H = constant value at σ at $\varepsilon_p=1$, n = strain hardening exponent, and E = Modulus of Elasticity.

Discussion

Structure and Hardness

The macrostructure and microstructure observation in the FSW joints shows that:

1. Even as a solid-state process, FSW produced enormous changes in the grain structure as well as in the plasma or fusion welded joints which have been observed in the weld regime. The grain size found also agreed with the results obtained by Benavides *et al.*, 1999, Booth and Sinclair, 2002, Sutton *et al.*, 2002 and Bussu and Irving, 2003 in which the oval N and FA exhibit finer grains (5 - 10 μm) than the parent plate (150 - 200 μm).

2. The severe elongated grain structure of the TMAZ which is about 200 - 400 μm was absent at the bottom of the weld surface since the size is narrow down through out the thickness of 10.5 mm of the plate from the top surface. It shows that the severe plastic deformation region is reduced when friction stir weld thick plate.

3. The N and FA exhibit the finest grain dimension and intermetallic particle distribution, whilst the TMAZ is coarsened which agreed with Flores *et al.*, 1998; Mahoney *et al.*, 1998; Jata and Semiatin, 2000; Jata *et al.*, 2000; Booth and Sinclair, 2002; Sutton *et al.*, 2002; Bussu and Irving, 2003, and Litynska *et al.*, 2003.

4. Due to the pin rotational direction, the asymmetrical micro-regime size in both the right and left sides was produced. This will lead to inhomogeneous macro mechanic properties with

respect to the weld and tool directions.

The hardness measurement on FSW joints indicate that:

1. The hardness of the top weld surface is higher than the bottom surface, which agreed with Bussu, 2000 and Heinz *et al.*, 2000. The lower hardness at the bottom surface is good for fatigue and that provides more ductility. The different hardness between the top and bottom is governed by the microstructural size, and strengthening precipitates distribution affected by the heat that causes overaging during the stir weld operation.

2. The maximum hardness (167 Hv1) has been observed within the HAZ, and the minimum (118 Hv1) in the TMAZ which is due to grain orientation and Cu precipitates distribution, rather than the grain size.

During welding the material undergoes frictional heating and stirring by the weld tool action from the top surface. High temperatures of 450 - 4,800°C (Dawes, 1995; Williams, 2001) combined with the stirring action allow thermo-mechanically-induced recrystallisation, which explains the presence of the fine grain observed in the N and FA. The elongated and bent grains in the TMAZ indicate a large amount of plastic deformation. Moreover, the through-thickness hardness gradient within the N would indicate the respective regions of material through the weld-thickness undergo different thermo-mechanical cycles. The asymmetry in size and hardness suggests that the regions of materials on the both sides of the PJJ undergo different thermo-mechanical cycles, with respect to pin rotation and weld directions. The drop in hardness in the fine grain regimes is believed to be governed by the precipitate's distribution, and TEM analysis would be required in order to establish the precipitate distribution and characteristic.

Residual Stress

Residual stress reveals an 'M'-like shape and is in agreement with residual stress measured in aluminium FSW joints reported in other works (Dalle Donne *et al.*, 2001; Webster *et al.*, 2001). Nevertheless, residual stresses measured from the top and bottom surfaces are different and are

due to absence of the TMAZ and FA regimes at the bottom surface. The TMAZ regime exhibits the maximum tensile residual stress (95 MPa). In the interpretation of the residual stress measurements it should be considered that, measuring two directions, the longitudinal and transverse residual stresses are not sufficient to satisfy the internal equilibrium, the perpendicular residual stress need to measure to complete description of the residual stress distribution across the weld. Furthermore, the layer removal technique gives an average longitudinal residual stresses reading compared with the hole drilling that provide a point or localised measurement. From a combination of both hole drilling and layer removal techniques, the residual stresses distribution in FSW is inhomogeneous and shows a gradient in the longitudinal direction as well as across the thickness of the weld. The TMAZ which comprises highly tensile residual stress is the best candidate to initiate a fatigue crack compared with N and TMAZ regimes that contain slightly compressive residual stresses.

Cyclic Deformation Behaviour

The material behaviour of each micro-structural regime of longitudinal FSW joints can be extracted from cyclic bending tests. It is important to understand that the loading history in fatigue is a cyclic type of loading. The HAZ, with the highest hardness, exhibits higher cyclic yielding point (410 MPa) whilst the TMAZ with the lowest hardness exhibit the lowest cyclic yielding point (250 MPa). This provides the information that yielding will take place at the first hardness minima (the TMAZ) and the expected fatigue failure within this regime. Due to a limited FSW bending sample, the complete cyclic stress-strain curve for the N regime could not be produced. However, the hardness in the N is higher than the hardness in the TMAZ and slightly lower than in the HAZ, giving us an idea that yielding might take place within the 320 - 350 MPa stress range.

Conclusions

1. The TMAZ seems to be a highly potential regime for where conventional crack

initiation will take place, specifically (a) high tensile residual stress, (b) low cyclic yield strength, (c) low hardness and (d) a highly elongated grain structure with coarsened in an inter-metallic particle distribution.

2. The strength and ductility of the weld micro-regime are controlled by the grain size and the presence of the coherent intragranular precipitates.

3. The residual stresses distribution is inhomogeneous and exhibits a gradient in the longitudinal direction and across the thickness.

4. The asymmetry in size, hardness, and residual stress within each micro-regime could be associated with the FSW processing attributes such as tool rotation direction, clamping forces, weld speed, weld direction, and friction forces that produced sufficient heat to weld the plate.

5. The critical area for fatigue can be determined by addressing the role of the micro and macro mechanic properties from the initiation stage to fracture.

6. The information from this characterisation work is useful for devising an engineer towards understanding the fatigue damage behaviour of FSW 2024-T351 Al Alloy joints.

Acknowledgement

The authors wish to thank Airbus UK for materials supply. A. Ali was sponsored for this study through a Malaysian Ministry of Science scholarship.

References

- Benavides, S., Li, Y., Murr, L.E., Brown, D., and McClure, J.C. (1999). Low temperature friction stir welding of 2024 Aluminum. *Scr.Mater.*, 41(8):809-815.
- Booth, D. and Sinclair, I. (2002). Fatigue of friction stir welded 2024-T351 Al-alloy. *Mater. Sci. Forum*, 396-402:1,671-1,676.
- Bussu, G. (2000). Damage tolerance of welded aluminum aircraft structure, [Ph.D. thesis]. Engineering Faculty, Cranfield University. UK, p. 287.
- Bussu, G. and Irving, P.E. (2003). The role of residual stress and heat affected zone

- properties on fatigue crack propagation in friction stir welded 2024-T351 Aluminum joints. *Int. J. Fatigue*, 25(1):77-88.
- Dawes, C.J. (1995). An introduction to friction stir welding and its development. *Welding & Metal Fabrication*, 63(1):13-16.
- Dalle Donne, C. and Biallas, G. (1999). Fatigue and fracture performance of friction stir welded 2024-T3. *Proceedings of the European Conference on Spacecraft Structure, Material and Mechanical Testing*, 1999; Nov 4-6, 1998; Braunschweig, Germany, 428:309-314.
- Dalle Donne, C., Lima, E., Wegener, J., Pyzalla, A., and Buslaps, T. (2001). Investigation on residual stress in friction stir welds. *Proceedings of 3rd International Symposium on Friction Stir Welding*; Sept 27-28, 2001; Kobe, Japan, TWI (UK), p. 281-291.
- Flores, O.V., Kennedy, C., Murr, L.E., Brown, D., Pappu, S., Nowak, B.M., and McClure, J.C. (1998). Microstructural issues in a friction stir welded aluminum alloy. *Scr. Mater.*, 38(5):703-708.
- Heinz, B., Skrotzki, B., and Eggeler, G.F. (2000). Microstructural and mechanical characterization of a friction stir welded Al-Alloy. *Mater. Sci. Forum*, 331-337:1,757-1,762.
- Jata, K.V., Sankaran, K.K., and Ruschau, J.J. (2000). Friction stir welding effects on microstructure and fatigue of aluminum alloy 7050-T7451. *Metall. Mater. Trans. A*, 31(9):2,181-2,192.
- Jata, K.V. and Semiatin, S.L. (2000). Continuous dynamic recrystallisation during friction stir welding of high aluminum alloys. *Scr. Mater.*, 43(8):743-749.
- Kwon, Y.J., Saito, N., and Shigematsu, I. (2002). Friction stir process as a new manufacturing technique of ultrafine grained aluminum alloy. *J. Mater. Sci. Lett.*, 21(19): 1,473-1,476.
- Litynska, L., Braun, R., Staniek, G., Dalle Donne, C., and Dutkiewicz, J. (2003). TEM study of the microstructure evolution in a friction stir welded AlCuMgAg alloy. *Mater. Chem. Phys.*, 81(2):293-295.
- Lu, J. (1996). *Handbook of Measurement of Residual Stresses*. 1st ed. Society for Experimental Mechanics, Inc. (SEM), Fairmont Press Inc., Litburn, GA, USA 238p.
- Mahoney, M.W., Rhodes, C.G., Flintoff, J.G., Bingel, W.H., and Spurling, R.A. (1998). Properties of friction stir welded 7075-T651 aluminum. *Metall. Mater. Trans. A*, 29(7): 1,955-1,964.
- Murr, L.E., Li, Y., Trillo, E.A., Flores, R.D., and McClure, J.C. (1998). Microstructure in friction stir welded metals. *J. Mater. Process. Manuf. Sci.*, 7:145-161.
- Nadai, A. (1950). *Theory of Flow and Fracture of Solids*. Vol. 1, 2nd ed. McGraw-Hill Inc, NY, USA, 527p.
- Sato, Y.S. and Kokawa, H. (2001). Distribution of tensile property and microstructure in friction stir weld of 6063 aluminum. *Metall. Mater. Trans. A*, 32(12):3,023-3,031.
- Sato, Y.S., Park, S.H.C., and Kokawa, H. (2001). Microstructure factors governing hardness in friction stir welds of solid solution hardened Al alloys. *Metall. Mater. Trans. A*, 32(12):3,033-3,042.
- Sutton, M.A., Yang, B., Reynolds, A.P., and Taylor, R. (2002). Microstructural studies of friction stir welds in 2024-T3 aluminum. *Mater. Sci. Eng. A*, 323(1):160-166.
- Webster, P.J., Oosterkamp, L.D., Browne, P.A., Hughes, D.J., Kang, W.P., Withers, P.J., and Vaughan, G.B.M. (2001). Synchrotron X-ray residual strain scanning of a friction stir weld. *J. Strain Anal. Eng. Des.*, 36(1): 61-70.
- Williams, S.W. (2001). Welding airframes using friction stir. *Air and Space Europe.*, 3:64-66.